

Testing the Organization of Whistler-mode Chorus Wave Properties by Plasmapause Location

David M. Malaspina¹, Allison N Jaynes², Scot R. Elkington¹, Anthony Arthur Chan³, George Blair Hospodarsky², and John Wygant⁴

¹University of Colorado Boulder

²University of Iowa

³Rice University

⁴University of Minnesota

November 26, 2022

Abstract

Lower-band whistler-mode chorus waves are important to the dynamics of Earth's radiation belts, playing a key role in accelerating seed population electrons (100's of keV) to relativistic (> 1 MeV) energies, and in scattering electrons such that they precipitate into the atmosphere. When constructing and using statistical models of lower-band whistler-mode chorus wave power, it is commonly assumed that wave power is spatially distributed with respect to magnetic L-shell. At the same time, these waves are known to drop in power at the plasmapause, a cold plasma boundary which is dynamic in time and space relative to L-shell. This study organizes wave power and propagation direction data with respect to distance from the plasmapause location to evaluate what role the location of the plasmapause may play in defining the spatial distribution of lower band whistler-mode chorus wave power. It is found that characteristics of the statistical spatial distribution of equatorial lower band whistler mode chorus are determined by L-shell, and are largely independent of plasmapause location. The primary physical importance of the plasmapause is to act as an Earthward boundary to lower band whistler mode chorus wave activity. This behavior is consistent with an equatorial lower band whistler mode chorus wave power spatial distribution that follows the L-shell organization of the particles driving wave growth.

Testing the Organization of Whistler-mode Chorus Wave Properties by Plasmapause Location

David M. Malaspina^{1,2}, Allison N. Jaynes³, Scot Elkington², Anthony Chan⁴,
George Hospodarsky³, John Wygant⁵

¹Department of Astrophysical and Planetary Sciences, University of Colorado, Boulder, Colorado, USA

²Laboratory for Atmospheric and Space Physics, University of Colorado, Boulder, Colorado, USA

³Department of Physics and Astronomy, University of Iowa, Iowa City, Iowa, USA

⁴Department of Physics and Astronomy, Rice University, Houston, Texas, USA

⁵School of Physics and Astronomy, University of Minnesota, Minneapolis, MN, USA

Key Points:

- An often-used assumption, that whistler-mode chorus properties are organized by L-shell, is tested and verified
- The plasmapause bounds whistler mode chorus activity but does not otherwise influence wave property distributions

Abstract

Lower-band whistler-mode chorus waves are important to the dynamics of Earth's radiation belts, playing a key role in accelerating seed population electrons (100's of keV) to relativistic (> 1 MeV) energies, and in scattering electrons such that they precipitate into the atmosphere. When constructing and using statistical models of lower-band whistler-mode chorus wave power, it is commonly assumed that wave power is spatially distributed with respect to magnetic L-shell. At the same time, these waves are known to drop in power at the plasmopause, a cold plasma boundary which is dynamic in time and space relative to L-shell. This study organizes wave power and propagation direction data with respect to distance from the plasmopause location to evaluate what role the location of the plasmopause may play in defining the spatial distribution of lower band whistler-mode chorus wave power. It is found that characteristics of the statistical spatial distribution of equatorial lower band whistler mode chorus are determined by L-shell, and are largely independent of plasmopause location. The primary physical importance of the plasmopause is to act as an Earthward boundary to lower band whistler mode chorus wave activity. This behavior is consistent with an equatorial lower band whistler mode chorus wave power spatial distribution that follows the L-shell organization of the particles driving wave growth.

Plain Language Summary

Whistler-mode chorus are plasma waves that can efficiently accelerate particles in Earth's radiation belts, and act to scatter them out of the radiation belts into Earth's atmosphere. Models of the statistical behavior of these plasma waves are important for predicting the shape of the radiation belts. For decades, wave models relied on the assumption that these particular waves are distributed in space similar to radiation belt particles - by distance from Earth at the magnetic equator. Another possibility is that the spatial distribution of these waves could be modified by the location of Earth's cold plasma torus, the plasmasphere. The plasmasphere moves toward and away from Earth on different time scales than radiation belt particles. This study tests how whistler-mode chorus plasma waves are organized in space, by comparing statistics of plasma wave properties organized by distance from the Earth at the magnetic equator with the same data organized by distance from the plasmasphere outer boundary. The long-standing assumption is found to be valid. This result is consistent with the interpretation that the spatial distribution of the plasma waves under study is determined by the spatial organization of the particles that drive the wave growth.

1 Introduction

Whistler-mode chorus waves are important to the dynamics of the Earth's radiation belts, playing a key role in accelerating seed population electrons (100's of keV) to relativistic (> 1 MeV) energies, (e.g. (Horne & Thorne, 1998; Summers et al., 1998; Horne et al., 2005; Reeves et al., 2013; Jaynes et al., 2015)) and in scattering electrons across a broad range of energies, often leading to their precipitation into the atmosphere (e.g. (Shprits et al., 2008; Thorne, 2010; Kasahara et al., 2018)).

In the inner terrestrial magnetosphere, whistler-mode chorus waves appear in two bands, a lower band ($0.1f_{ce} < f < 0.5f_{ce}$), and an upper band, ($0.5f_{ce} < f < f_{ce}$), where f_{ce} is the electron cyclotron frequency (e.g. (Burtis & Helliwell, 1969; Tsurutani & Smith, 1977; Santolík et al., 2003)). Also, in this region, whistler-mode chorus waves are driven by cyclotron resonance with electron distributions with strong perpendicular temperature anisotropy (Schriver et al., 2010; Li et al., 2010; Lee et al., 2014), generated as electrons are adiabatically transported Earthward via impulsive injections from the plasma sheet during geomagnetic storms and substorms (e.g. (Sazhin & Hayakawa, 1992)).

65 A large number of studies have examined the spatial distribution of whistler-mode
 66 chorus wave power as a function of L-shell, MLT, and geomagnetic indices, demonstrat-
 67 ing that the highest mean wave amplitudes occur in the dawn sector (where injected elec-
 68 trons gradient-curvature drift about the Earth), near the equator (where the strongest
 69 adiabatic temperature anisotropy occurs), and at L-shells of ~ 7 (e.g. (Tsurutani & Smith,
 70 1977; Meredith et al., 2001, 2003; Bortnik et al., 2007; Cully et al., 2008; Li et al., 2009,
 71 2010, 2011; Meredith et al., 2012; Li et al., 2016; O. V. Agapitov et al., 2015; Meredith
 72 et al., 2018)). Several of these studies have demonstrated, using case studies of individ-
 73 ual plasmopause crossings, that the plasmopause (the outer boundary of the plasmas-
 74 sphere, the cold dense plasma torus about Earth) constitutes an Earthward boundary to
 75 chorus wave activity (e.g. (Meredith et al., 2001)). The drop off of whistler-mode cho-
 76 rus wave power at the plasmopause is starkly visible in statistical wave power studies
 77 when chorus wave power near the geomagnetic equator is organized by distance from the
 78 plasmopause (Malaspina et al., 2016).

79 While the drop in equatorial whistler-mode chorus wave power at the plasmopause
 80 is well documented by case study observations, nearly all statistical studies of the spa-
 81 tial distribution of whistler-mode chorus power use the plasmopause only as an inner bound-
 82 ary for the identification of whistler-mode chorus waves (e.g. (Meredith et al., 2012; Li
 83 et al., 2016)). In these studies, wave property statistics are parameterized by L-shell, MLT,
 84 and geomagnetic indices, effectively averaging over many plasmopause radial locations
 85 and 'smoothing away' the physical drop in whistler-mode wave power at the plasmopause.
 86 This smoothing effect can be particularly strong because the plasmopause is dynamic
 87 in time and space with respect to L-shell. Plasmopause location varies in time through
 88 a wide range of L-shells (2 - 7) as a function of geomagnetic conditions, MLT, and the
 89 time history of both the solar wind convection electric field and ionospheric refilling (Carpenter
 90 & Lemaire, 2004).

91 This raises a question: to what extent does the spatial distribution of near-equatorial
 92 whistler-mode chorus wave power depend upon the plasmopause location? For exam-
 93 ple, the above-referenced studies examining the spatial distribution of whistler-mode cho-
 94 rus wave power all report a gradual drop in lower band whistler-mode wave power Earth-
 95 ward of $L = 7$. Is this a physical feature of the chorus wave spatial distribution or an
 96 artifact of smoothing wave statistics over variable plasmopause locations?

97 For a different whistler-mode wave in the inner magnetosphere, plasmaspheric hiss,
 98 the shape, location, and density profile of the plasmasphere strongly determine the wave
 99 power spatial distribution (Malaspina et al., 2016, 2017, 2018). For hiss, wave power mod-
 100 ulation by plasmaspheric structure is thought to be largely a consequence of wave refrac-
 101 tion, which is highly sensitive to the distribution of cold plasma density ((Maxworth &
 102 Gołkowski, 2017) and references therein). In contrast, the whistler-mode chorus source
 103 region and typical propagation regions are in general well outside the plasmopause (Bortnik
 104 et al., 2006; Chen et al., 2013), so the plasmasphere may have a weaker effect on cho-
 105 rus wave power distributions.

106 This work aims to quantify the impact of plasmopause location on the spatial dis-
 107 tribution of near-equatorial lower band whistler-mode chorus wave properties. To do so,
 108 observations of whistler-mode chorus wave properties are compiled and organized by the
 109 location of the plasmopause with respect to Earth (L_{pp}), distance from the plasmopause
 110 (ΔL_{pp}), and magnetic local time (MLT). These statistics are then compared against wave
 111 property statistics organized using L-shell, L_{pp} , and MLT. In this study, the wave data
 112 are not explicitly parameterized by geomagnetic indices, though the geomagnetic activ-
 113 ity level is implicitly included through L_{pp} .

114 Quasi-linear diffusion models of radiation belt dynamics typically ingest statisti-
 115 cal models of wave power organized by L-shell, geomagnetic indices, and MLT (Subbotin
 116 & Shprits, 2009; Fok et al., 2011; Horne et al., 2013; Orlova et al., 2014; Glauert et al.,

117 2014). This work quantitatively tests an assumption commonly used in these models:
 118 that parameterization by L-shell is the most physically appropriate description of the
 119 chorus wave spatial distribution.

120 2 Data Set and Processing

121 This work uses data from the Van Allen Probes mission. These twin spacecraft were
 122 launched in August of 2012 and were de-orbited in 2019. During their mission, they or-
 123 bited Earth between 600 km altitude and ~ 6 Earth radii. They were spin stabilized, ro-
 124 tating once every ~ 11 s, orbiting Earth every ~ 9 hours, and precessing through all lo-
 125 cal times every ~ 2 years. Their orbits covered $\pm 20^\circ$ of the magnetic equator. The in-
 126 struments used in this analysis are the Electric and Magnetic Field Instrument Suite and
 127 Integrated Science (EMFISIS) (Kletzing et al., 2013) and the Electric Fields and Waves
 128 (EFW) instrument (Wygant et al., 2013).

129 This work examines lower band whistler-mode chorus wave power, wave normal an-
 130 gle, and Poynting flux direction as a function of parameters including: spacecraft L-shell
 131 location (L), distance between the spacecraft and the plasmopause in units of L-shell (ΔL_{pp}),
 132 and the distance of the plasmopause from Earth (L_{pp}).

133 The TS04D magnetic field model (Tsyganenko & Sitnov, 2005) is used to define
 134 L , ΔL_{pp} , and L_{pp} for each wave power observation. The specific L definition used here
 135 is McIlwain L-shell (McIlwain, 1961) for 90 degree pitch angle particles. Cold plasma den-
 136 sity is estimated using the spacecraft floating potential data calibrated each day against
 137 densities determined via the upper hybrid resonance line, as in (Malaspina et al., 2016).
 138 Following (Moldwin et al., 2002), plasmopause crossings are identified as the most Earth-
 139 ward sharp density gradient (more than 5x change in density over 0.5 L-shell) on a given
 140 inbound or outbound pass of the spacecraft. The quantity ΔL_{pp} is defined as $L - L_{pp}$,
 141 where L_{pp} is the plasmopause location determined on a given outbound or inbound pass
 142 of the spacecraft. Data from passes without an identified plasmopause crossing are ex-
 143 cluded in this work.

144 Wave power is determined using the EMFISIS survey power spectra of signals from
 145 the three search coil magnetometer (SCM) axes, as calculated on-board. These on-board
 146 calculated spectra capture 0.5 seconds of data every 6 seconds, producing power spec-
 147 tral densities between ~ 2 Hz and ~ 12 kHz in 65 pseudo-logarithmically spaced frequency
 148 bins. Lower-band whistler-mode chorus wave power for a given spectra is determined by
 149 summing the power spectral densities from all three SCM axes, multiplying by the band-
 150 width of each frequency bin, and summing data from $0.1f_{ce}$ to $0.5f_{ce}$. Here f_{ce} is the
 151 electron cyclotron frequency local to each spectral observation, determined using the mag-
 152 netic field magnitude as measured by the fluxgate magnetometer.

153 Using SCM wave power data for this study instead of electric field wave data avoids
 154 complications associated with nonlinear electrostatic structure wave power in whistler-
 155 mode frequency bands (Mozer et al., 2013) as well as those associated with non-uniform
 156 sensor response along different measurement axes (Hartley et al., 2016). In SCM data,
 157 whistler-mode chorus are well-isolated narrow band (on a logarithmic scale) waves. Spec-
 158 tral bins dominated by magnetosonic waves are excluded using the following criteria on
 159 compressibility: $B_{\parallel} / B_{\perp} < 0.6$. Here, B_{\parallel} is the magnetic field wave amplitude paral-
 160 lel to the background magnetic field and B_{\perp} is the magnetic field wave amplitude per-
 161 pendicular to the background magnetic field, in a given spectral frequency bin. Data recorded
 162 during times of strong spacecraft charging, eclipse, and thruster firings are excluded from
 163 consideration. Data where the signal to noise ratio was less than 5 were excluded from
 164 consideration, where the SCM noise level definition from (Malaspina et al., 2017) was
 165 used.

166 This study also makes use of wave normal direction and Poynting flux direction for
 167 lower band whistler-mode chorus. Both quantities are derived from EMFISIS on-board
 168 cross-spectral data. Specifically examined in this study are (i) θ_{kB} , the polar angle be-
 169 tween the wave normal vector direction and the background magnetic field, and (ii) θ_{SB} ,
 170 the polar angle between the Poynting flux direction and the background magnetic field.
 171 Valid θ_{kB} values range from 0 (parallel/anti-parallel with \vec{B}) to 90 (perpendicular to \vec{B}).
 172 Valid θ_{SB} values range from 0 (parallel to \vec{B}) to 180 (anti-parallel to \vec{B}). θ_{kB} angles are
 173 calculated using the single value decomposition (SVD) analysis method (Santolík et al.,
 174 2003) applied to only the three axis SCM wave data. SVD-method wave normal angle
 175 determination was considered to be valid for frequency/time bins with planarity > 0.5 ,
 176 ellipticity > 0.5 and coherence between the two SCM signals orthogonal to the back-
 177 ground magnetic field > 0.5 . These quantities and their derivations are detailed in (Santolík
 178 et al., 2003).

179 The lower band whistler-mode chorus wave band can only be fully captured when
 180 $0.5 f_{ce}$ is below the upper frequency limit of the EMFISIS on-board power spectra (12
 181 kHz). This condition is generally satisfied for $L > 3.5$. Closer to Earth than $L = 3.5$,
 182 prior studies indicate (e.g. (Meredith et al., 2018) and references therein), that lower band
 183 whistler-mode chorus wave power near the magnetic equator is often negligibly small,
 184 though this condition can be violated during periods of high geomagnetic activity. Lower
 185 band whistler-mode chorus wave power Earthward of the plasmopause, near the mag-
 186 netic equator, is considered to be negligible in this study.

187 Data recorded by the Van Allen Probes between October 1, 2012 and March 31,
 188 2018 were used in this study, encompassing nearly three full precessions of the orbit through
 189 all local times. Data from Van Allen Probe A after May of 2016 were not used because,
 190 in approximately June of 2016, radiation damage to preamplifier electronics degraded
 191 the spacecraft potential measurement on Van Allen Probe A to the point where it was
 192 not useful for density determination.

193 2.1 Analysis

194 Figure 1 shows data from one orbit of Van Allen Probe B on 01 September, 2014
 195 when the orbit apogee was near dawn. Figure 1a shows the derived cold plasma density,
 196 with vertical red dashed lines indicating the identified plasmopause crossings on the in-
 197 bound and outbound legs of the orbit. Between 14:00 and 16:00 UTC, a weak spacecraft
 198 charging event influenced the plasma density estimate. Figure 1b shows the total power
 199 spectral density from the two components of the electric field measured in the spacecraft
 200 spin plane. The frequencies $0.5 f_{ce}$ and $0.1 f_{ce}$ are overlaid in white solid lines, f_{ce} is shown
 201 as a dashed white line. Broadband signals corresponding to kinetic electric field struc-
 202 tures such as phase space holes and kinetic Alfvén waves pervade the electric field wave
 203 data (Mozer et al., 2013; Chaston et al., 2015), especially near 11:00 and 15:00 UTC. Fig-
 204 ure 1c shows the total power spectral density from all three SCM axes. Plasmaspheric
 205 hiss is observed Earthward of the plasmopause on both legs of the orbit, between ~ 150
 206 Hz and 2 kHz on the outbound leg and between ~ 50 Hz and 2 kHz on the inbound leg.
 207 Figure 1d shows the band-integrated ($0.1 f_{ce}$ to $0.5 f_{ce}$) lower-band whistler-mode mag-
 208 netic field wave power. Lower-band whistler-mode wave power is located outside the plas-
 209 masphere, between $0.1 f_{ce}$ and $0.5 f_{ce}$, and is well-separated in frequency from other wave
 210 modes in the SCM data. While the lower-band whistler-mode waves show extended pe-
 211 riods of activity, the variation in wave power during those periods can be as high as four
 212 orders of magnitude. This behavior is typical of whistler mode chorus (Santolík et al.,
 213 2010, 2014).

214 To compare lower-band whistler-mode properties under L-shell parameterization
 215 with those same properties under ΔL_{pp} parameterization, statistics of wave power, θ_{kB} ,
 216 and θ_{SB} are presented. The full data set, after the exclusions described in the prior sec-

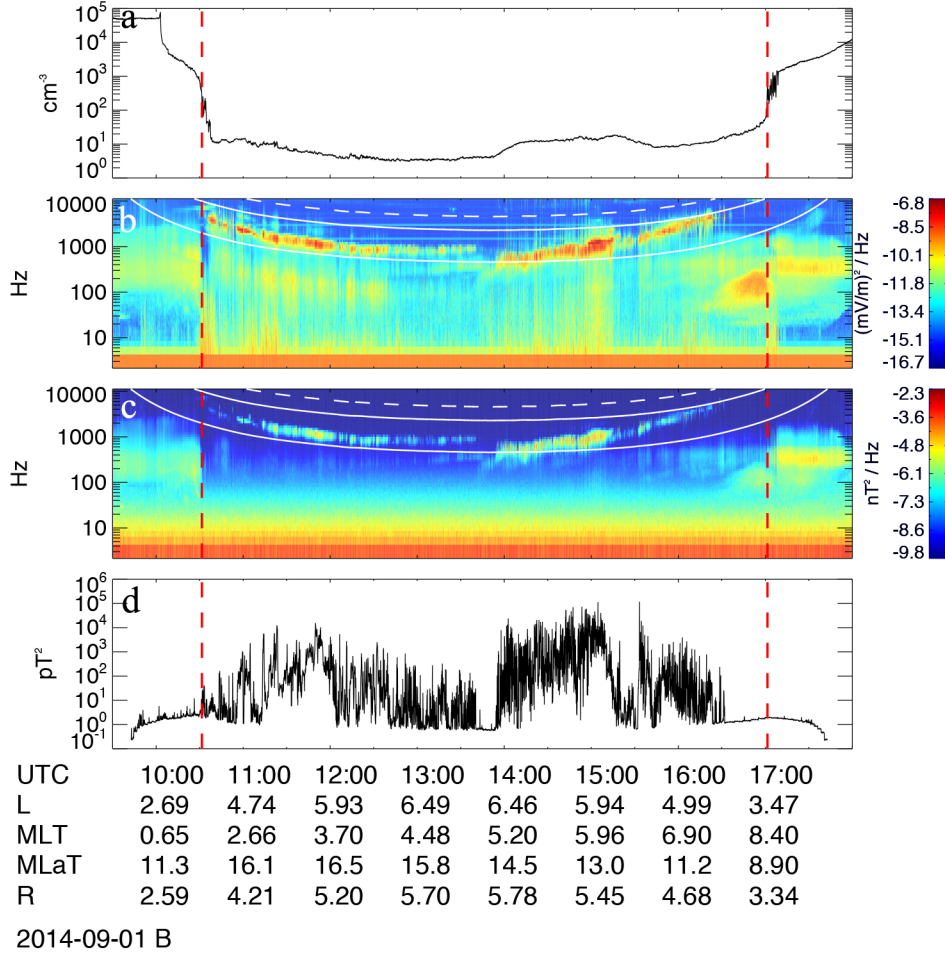


Figure 1. Plasma waves and density variation during one orbit of Van Allen Probe B on 01 September, 2014. (a) Plasma density derived from the spacecraft floating potential calibrated against the upper hybrid resonance line, (b) spectrogram of electric field wave power, (c) spectrogram of magnetic field wave power, (d) band-integrated wave power during this interval between 0.1 and 0.5 times the electron cyclotron frequency. Dashed white lines in (b) and (c) indicate the electron cyclotron frequency (f_{ce}) and solid white lines indicate $0.5f_{ce}$ and $0.1f_{ce}$.

217 tion, consists of $\sim 3.12 \times 10^7$ 0.5 s samples of lower-band whistler-mode waves distributed
 218 across L-shell, MLT, and geomagnetic activity level.

219 Wave property statistics are divided into four MLT sectors: Dawn ($3 < MLT < 9$), Noon ($9 < MLT < 15$), Dusk ($15 < MLT < 21$), and Midnight ($21 < MLT < 24$
 220 and $0 < MLT < 3$). The statistics are also divided into four bins based on the loca-
 221 tion of the plasmapause with respect to Earth: $2 < L_{pp} < 3$, $3 < L_{pp} < 4$, $4 < L_{pp} < 5$, and $5 < L_{pp} < 6$. The geomagnetic activity is convolved with this binning, as
 222 heavily eroded plasmaspheres occur when geomagnetic activity is high, and extended plas-
 223 maspheres occur when geomagnetic activity is low.
 224
 225

226 Figure 2 shows histograms of lower-band whistler-mode wave occurrence as a func-
 227 tion of wave power and L-shell for data recorded in the Dawn sector ($3 < MLT < 9$).
 228 Plots in the left column show data organized by L-shell, while plots in the right column

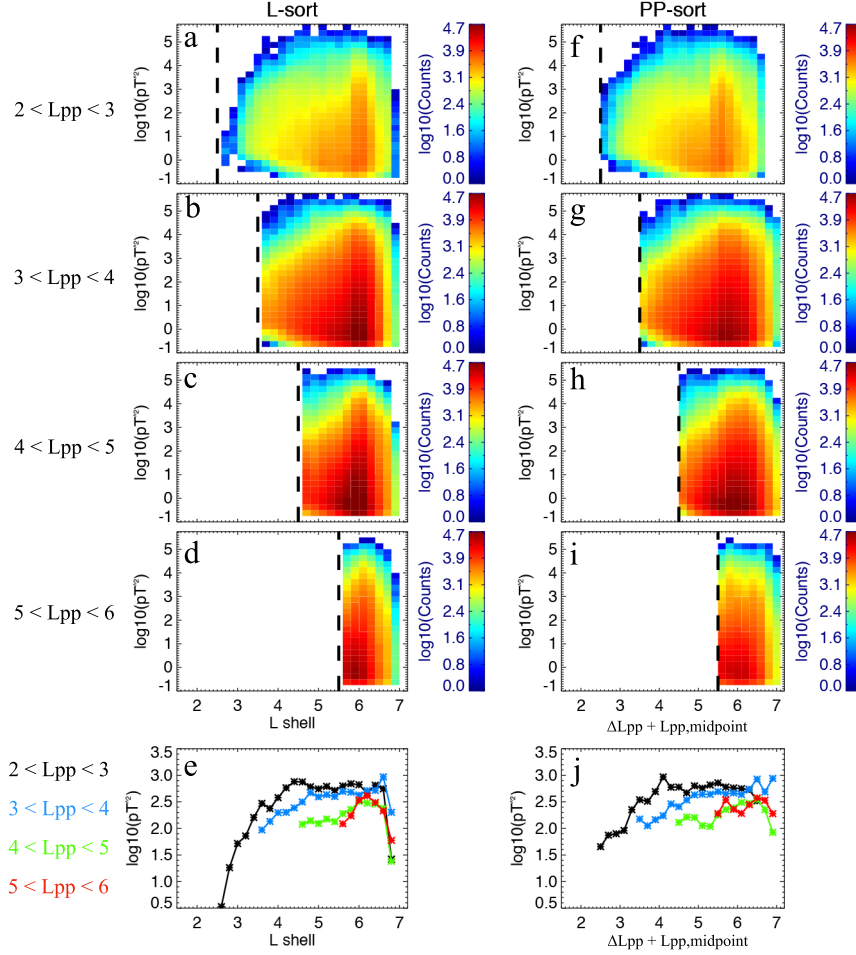


Figure 2. Histograms of lower-band whistler-mode wave occurrence as a function of wave power and L-shell for (a,b,c,d) data organized by L-shell and (f,g,h,i) data organized by distance to the plasmopause, shifted by the midpoint plasmopause location ($\Delta L_{pp} + L_{pp,midpoint}$), so that the data are directly comparable to (a,b,c,d). (a,f) data for plasmopause locations between $L = 2$ and $L = 3$, (b,g) data for plasmopause locations between $L = 3$ and $L = 4$, (c,h) data for plasmopause locations between $L = 4$ and $L = 5$, (d,i) data for plasmopause locations between $L = 5$ and $L = 6$. (e,j) Mean wave power as a function of L-shell derived from the distributions in (a,b,c,d) and (f,g,h,i).

229 show data organized by distance from the plasmopause, shifted by the value of L_{pp}
 230 at the midpoint of the plasmopause location bin ($L_{pp,midpoint} = 2.5, 3.5, 4.5$, etc.). This
 231 shift enables the plasmopause-sorted data to be directly compared with the L-sort data.
 232 The top row shows data where $2 < L_{pp} < 3$, the second row data where $3 < L_{pp} < 4$,
 233 the third row data where $4 < L_{pp} < 5$, and the fourth row data where $5 < L_{pp} < 6$.
 234 In each case, $L_{pp,midpoint}$ is indicated by a vertical dashed black line.

235 We choose not to collapse over the wave amplitude dimension when displaying these
 236 statistics because whistler-mode chorus wave amplitude distributions are known to be
 237 heavily tailed (Watt et al., 2017), with the probability of observing a particular ampli-
 238 tude decreasing toward higher amplitudes.

239 The bottom row shows the mean wave power per L-shell bin for each L_{pp} condi-
 240 tion: black = $2 < L_{pp} < 3$, blue = $3 < L_{pp} < 4$, green = $4 < L_{pp} < 5$, and red =
 241 $5 < L_{pp} < 6$. While taking the mean collapses the amplitude dimension, mean wave
 242 power is often the most relevant quantity for quasi-linear representations of radiation belt
 243 modeling (Subbotin & Shprits, 2009; Fok et al., 2011; Horne et al., 2013; Orlova et al.,
 244 2014; Glauert et al., 2014).

245 The most striking feature of Figure 2 is the strong similarity between the left and
 246 right columns. Independent of whether the data are organized by L-shell or ΔL_{pp} , the
 247 highest amplitude waves are most likely to occur near $L = 6$, and the likelihood of ob-
 248 serving high amplitude waves falls toward Earth. This trend persists for all L_{pp} bins. The
 249 overall shape of the amplitude/L-shell wave power distribution remains the same as L_{pp}
 250 varies, for both the L-sorted data and the ΔL_{pp} -sorted data. The only impact of L_{pp} vari-
 251 ation is to set the Earthward cutoff of an otherwise weakly changing (in L-shell) distri-
 252 bution.

253 The two panels in the bottom row show that the mean wave amplitudes drop to-
 254 ward Earth, and they drop as L_{pp} increases, consistent with an overall change in geo-
 255 magnetic activity. The drop in mean wave power beyond $L \approx 6.5$ occurs because the
 256 Van Allen Probes' orbital apogee rarely exceeds this value and the statistical coverage
 257 of these high-L bins is poor. The data in Figure 2e and Figure 2j are compared directly
 258 in Figure 5.

259 Figure 3 has a similar format to Figure 2, except that the quantity examined is θ_{kB} ,
 260 the angle between the SVD-determined wave normal vector and the background mag-
 261 netic field vector. Two distinct populations are present, a quasi-field aligned population
 262 with $\theta_{kB} < 30^\circ$, and an oblique population with $50^\circ < \theta_{kB} < 80^\circ$. The two pop-
 263 ulations separate more distinctly closer to Earth, and merge for $5 < L < 6$, the dis-
 264 tance where the strongest wave amplitudes also occur. The wave normal angles of lower-
 265 band whistler-mode waves in the radiation belt are often well-described in terms of cold
 266 plasma theory, and have been examined extensively in other works (e.g. (Hartley et al.,
 267 2015; Li et al., 2016; O. V. Agapitov et al., 2016)).

268 The bottom row shows the peak value of the θ_{kB} distributions as a function of L-
 269 shell for the portion of the distribution where $\theta_{kB} < 45^\circ$. The data in Figure 3e and
 270 Figure 3j are compared directly in Figure 5.

271 The feature of interest for this study is, again, how similar the L-sorted data (left
 272 column) are to the ΔL_{pp} -sorted data (right column). The spatial morphology of the θ_{kB}
 273 distributions exterior to the plasmopause appear to be approximately static in L-shell
 274 as the plasmopause location varies. The portions of the distribution Earthward of the
 275 plasmopause are removed in response to outward motion of the plasmopause.

276 Figure 4 has the same format as Figure 3, and the quantity examined is θ_{SB} , the
 277 angle between the wave Poynting vector and the background magnetic field vector.

278 One population approximately parallel to \vec{B} , and one population approximately
 279 anti-parallel to \vec{B} , are present. The two populations are separated at all distances from
 280 Earth, but least so for $5 < L < 6$, the distance where the strongest wave amplitudes
 281 also occur. The parallel and anti-parallel populations of whistler-mode chorus near the
 282 magnetic equator have been well-documented and interpreted as whistler-mode chorus
 283 moving away from a magnetic equator source region (e.g. (Santolík et al., 2005; O. Agapi-
 284 tov et al., 2010)). As with wave power and θ_{kB} , the θ_{SB} distributions are strongly sim-
 285 ilar between the L-sorted data and ΔL_{pp} -sorted data.

286 The bottom row shows the peak (most likely to be observed) θ_{SB} value as a func-
 287 tion of L-shell for the portion of the distribution where $\theta_{SB} < 45^\circ$. The data in Fig-
 288 ure 4e and Figure 4j are compared directly in Figure 5.

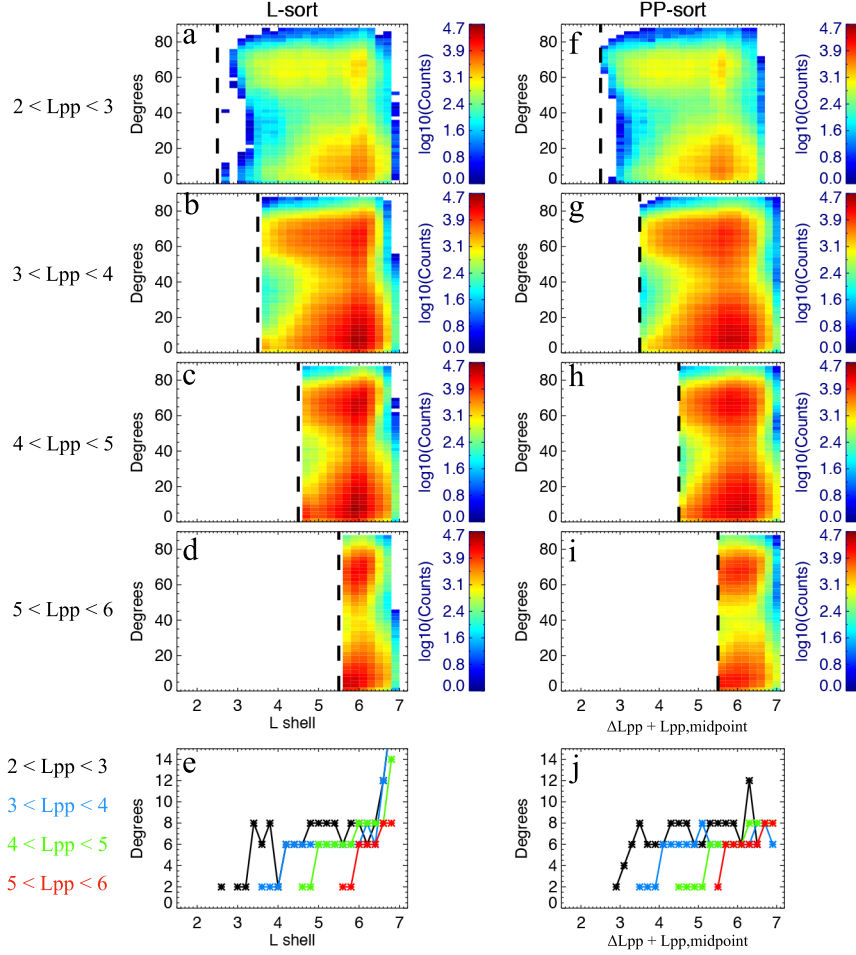


Figure 3. Same format as Figure 2, but for the quantity θ_{kB} . (e,j) Peak value of θ_{kB} for $\theta_{kB} < 45^\circ$ as a function of L-shell, for the distributions in (a,b,c,d) and (f,g,h,i).

289 Plots similar to Figure 2, Figure 3, and Figure 4, but for the other three quadrants
 290 (Noon, Dusk, Midnight) are included in the supplementary material. Each of these plots
 291 show the same behavior, in that (i) the L-shell and ΔL_{pp} distributions are strikingly similar,
 292 and (ii) the plasmopause acts to truncate the distribution toward Earth, but does
 293 not strongly influence other characteristics of the distribution (e.g. L-shell location of
 294 the largest amplitude waves).

295 3 Discussion

296 Figure 5 shows comparisons between the mean wave power (left column), peak θ_{kB}
 297 below 45° (center column), and peak θ_{SB} below 45° (right column) for L-sorted data (black
 298 traces) and ΔL_{pp} -sorted data (red traces, with x-axis of $\Delta L_{pp} + L_{pp, \text{midpoint}}$). The four
 299 rows (top to bottom) show data for $2 < L_{pp} < 3$, $3 < L_{pp} < 4$, $4 < L_{pp} < 5$, and
 300 $5 < L_{pp} < 6$. These data are from the Dawn sector, and correspond to the data plotted
 301 in the bottom rows of Figures 2, 3, and 4. In all cases, there is close agreement between
 302 the L-sort and ΔL_{pp} -sort traces.

303 Small ($< 0.5L$) offsets are present, due to the $1L$ finite width of the L_{pp} bins. When
 304 translating the ΔL_{pp} -sorted data onto an L-shell-based x-axis, the bin-middle $L_{pp, \text{midpoint}}$

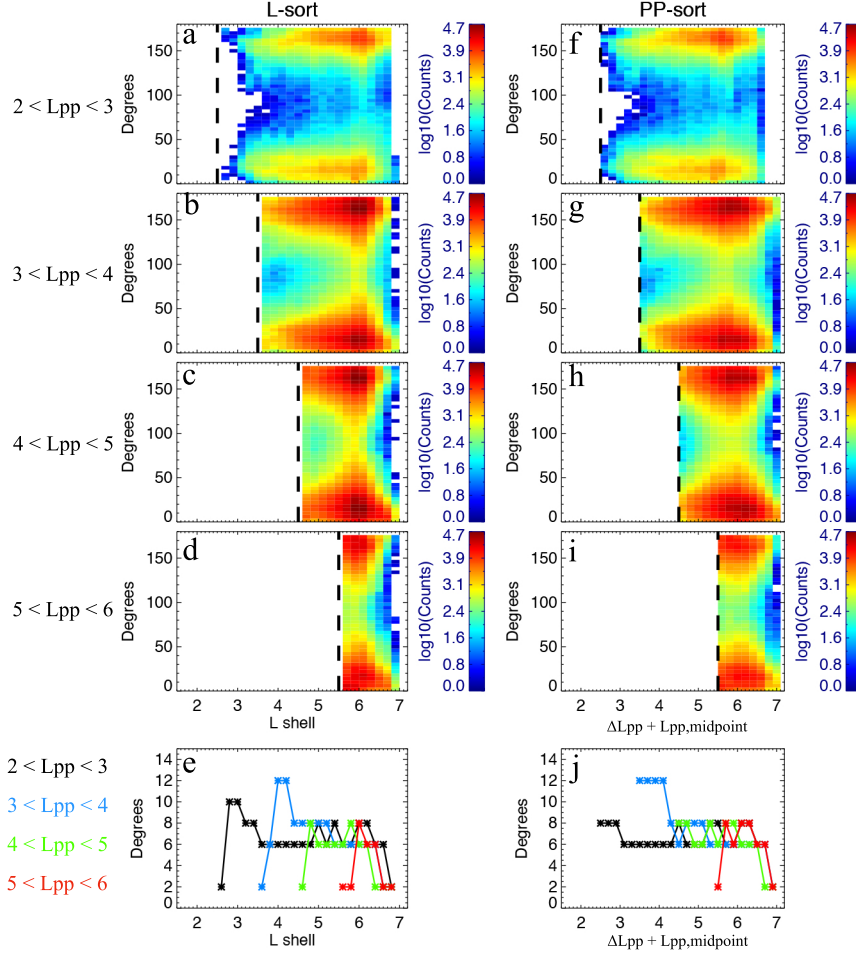


Figure 4. Same format as Figure 2, but for the quantity θ_{SB} . (e,j) Peak value of θ_{SB} for $\theta_{SB} < 45^\circ$ as a function of L-shell, for the distributions in (a,b,c,d) and (f,g,h,i).

305 value was used (e.g. $L_{pp,midpoint} = 2.5$ for $2 < L_{pp} < 3$). This can introduce a small
 306 offset in L-shell when the distribution of L_{pp} values in a given L_{pp} bin is skewed more
 307 toward the high end of the bin (as with $2 < L_{pp} < 3$).

308 The preceding analyses demonstrate that the distributions of lower band whistler
 309 mode chorus wave power, θ_{kB} and θ_{SB} retain a similar shape and spatial organization
 310 with respect to L-shell outside of the plasmopause, whether or not organization with re-
 311 spect to plasmopause position is considered. This is true even for locations close to the
 312 plasmopause. This result indicates that the primary role of the plasmopause in shaping
 313 the statistical spatial distribution of equatorial lower band whistler mode chorus wave
 314 properties is to define an Earthward boundary for wave activity.

315 This behavior is markedly different from plasmaspheric hiss, where the plasmas-
 316 pheric density profile (Breneman et al., 2015; Malaspina et al., 2018) and plasmopause
 317 location (Malaspina et al., 2016) strongly determine the hiss wave power distribution.
 318 The differing behaviors of chorus and hiss spatial distributions are consistent with: (i)
 319 an equatorial lower band whistler mode chorus wave power spatial distribution that is
 320 co-located with the L-shell organization of particles driving wave growth (in agreement
 321 with prior studies such as (Li et al., 2010; Lee et al., 2014)) and, (ii) an equatorial plas-

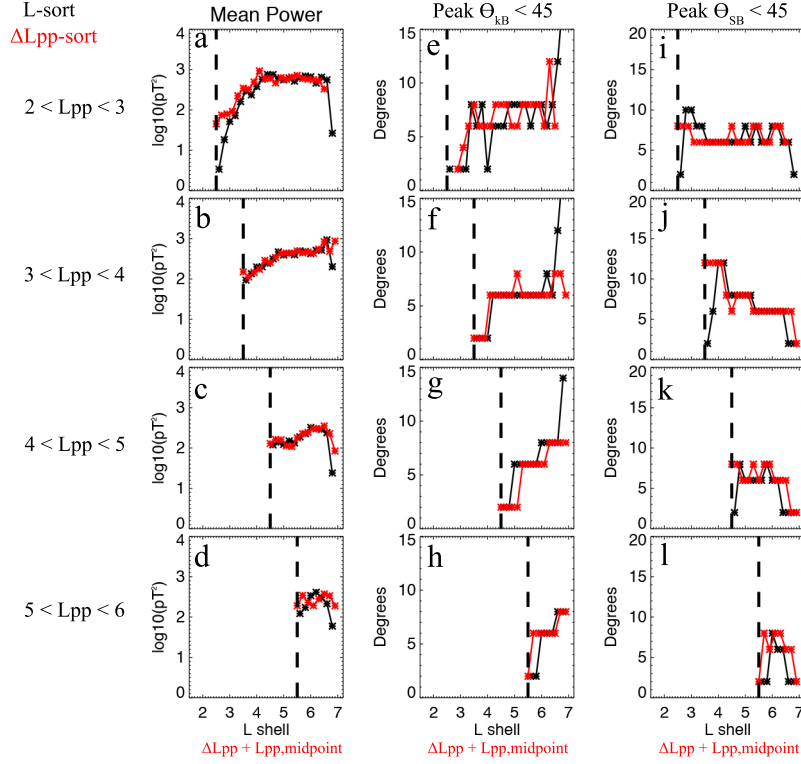


Figure 5. Comparison between wave mean power (left column), θ_{kB} (middle column), and θ_{SB} (right column) for L-sorted wave data (black traces) and $\Delta L_{pp} + L_{pp,midpoint}$ -sorted data (red traces). (a,e,i) data for plasmopause locations between $L = 2$ and $L = 3$, (b,f,j) data for plasmopause locations between $L = 3$ and $L = 4$, (c,g,k) data for plasmopause locations between $L = 4$ and $L = 5$, (d,h,l) data for plasmopause locations between $L = 5$ and $L = 6$.

322 maspheric hiss wave power spatial distribution that is determined by whistler-mode prop-
 323 agation effects and consequently, the refractive properties of the plasma within the plas-
 324 masphere (Chen et al., 2012; Malaspina et al., 2018). One exception to this dichotomy
 325 is low frequency hiss ($< 150Hz$), which has been shown to be co-located with the par-
 326 ticles driving its wave growth (Shi et al., 2017).

327 4 Conclusions

328 Understanding the spatial distribution of equatorial lower band whistler-mode cho-
 329 rus wave power statistically is important for our understanding of radiation belt dynam-
 330 ics, in that whistler-mode waves play a significant role in both relativistic electron ac-
 331 celeration and electron scattering. It is well-understood from prior observations that whistler-
 332 mode chorus wave power drops at the plasmopause, but the plasmopause is a dynamic
 333 boundary in both space and time with respect to L-shell.

334 The goal of this study was to compare statistical distributions of lower band whistler-
 335 mode chorus wave properties using L-shell sorting and plasmopause-based sorting of the
 336 data. The primary result is that the plasmopause location does not play a strong role
 337 in shaping the statistical spatial distribution of equatorial lower band whistler mode cho-
 338 rus outside of the plasmopause. In the Van Allen Probes data, whistler-mode chorus mean

339 wave amplitudes peak near the apogee of the Van Allen Probes orbit and fall Earthward
340 of that location, regardless of whether the plasmopause location is considered.

341 The lack of systematic difference between the data when sorted by L-shell or by
342 distance from the plasmopause supports the long-used assumption that equatorial lower
343 band whistler mode chorus wave properties are physically organized by L-shell. There-
344 fore, quasi-linear diffusion models of radiation belt dynamics are expected to produce
345 similar results whether they use L-sorted data or plasmopause-sorted data for lower band
346 whistler mode chorus waves.

347 Acknowledgments

348 The authors thank the Van Allen Probes team, especially the EFW and EMFISIS
349 teams for their support. This work was funded by NASA award NNX17AI51G. All Van
350 Allen Probes data used in this work are available from the EFW and EMFISIS team web-
351 sites, which one can link to here: <http://rbsp.gway.jhuapl.edu>. The authors acknowledge
352 the International Space Sciences Institute (ISSI) and the participants in a 2020 ISSI work-
353 shop in Bern.

354 References

- 355 Agapitov, O., Krasnoselskikh, V., Zaliznyak, Y., Angelopoulos, V., Le Contel, O.,
356 & Rolland, G. (2010, June). Chorus source region localization in the Earth's
357 outer magnetosphere using THEMIS measurements. *Annales Geophysicae*,
358 *28*(6), 1377-1386. doi: 10.5194/angeo-28-1377-2010
- 359 Agapitov, O. V., Artemyev, A. V., Mourenas, D., Mozer, F. S., & Krasnoselskikh,
360 V. (2015, December). Empirical model of lower band chorus wave distribution
361 in the outer radiation belt. *Journal of Geophysical Research (Space Physics)*,
362 *120*, 10. doi: 10.1002/2015JA021829
- 363 Agapitov, O. V., Mourenas, D., Artemyev, A. V., & Mozer, F. S. (2016, November).
364 Exclusion principle for very oblique and parallel lower band chorus waves. *Geo-
365 physical Research Letters*, *43*(21), 11,112-11,120. doi: 10.1002/2016GL071250
- 366 Bortnik, J., Inan, U. S., & Bell, T. F. (2006, February). Landau damping and resul-
367 tant unidirectional propagation of chorus waves. *Geophysical Research Letters*,
368 *33*, L03102. doi: 10.1029/2005GL024553
- 369 Bortnik, J., Thorne, R. M., & Meredith, N. P. (2007, August). Modeling the
370 propagation characteristics of chorus using CRRES suprathermal electron
371 fluxes. *Journal of Geophysical Research (Space Physics)*, *112*, A08204. doi:
372 10.1029/2006JA012237
- 373 Breneman, A. W., Halford, A., Millan, R., McCarthy, M., Fennell, J., Sample, J.,
374 ... Kletzing, C. A. (2015, July). Global-scale coherence modulation of
375 radiation-belt electron loss from plasmaspheric hiss. *Nature*, *523*, 193-195.
376 doi: 10.1038/nature14515
- 377 Burtis, W. J., & Helliwell, R. A. (1969). Banded chorus-A new type of VLF radi-
378 ation observed in the magnetosphere by OGO 1 and OGO 3. *Journal of Geo-
379 physical Research*, *74*, 3002. doi: 10.1029/JA074i011p03002
- 380 Carpenter, D., & Lemaire, J. (2004, December). The Plasmasphere Boundary Layer.
381 *Annales Geophysicae*, *22*, 4291-4298. doi: 10.5194/angeo-22-4291-2004
- 382 Chaston, C. C., Bonnell, J. W., Kletzing, C. A., Hospodarsky, G. B., Wygant, J. R.,
383 & Smith, C. W. (2015, October). Broadband low-frequency electromagnetic
384 waves in the inner magnetosphere. *Journal of Geophysical Research (Space
385 Physics)*, *120*, 8603-8615. doi: 10.1002/2015JA021690
- 386 Chen, L., Li, W., Bortnik, J., & Thorne, R. M. (2012, April). Amplification of
387 whistler-mode hiss inside the plasmasphere. *Geophysical Review Letters*, *39*,
388 L08111. doi: 10.1029/2012GL051488

- 389 Chen, L., Thorne, R. M., Li, W., & Bortnik, J. (2013, March). Modeling the wave
390 normal distribution of chorus waves. *Journal of Geophysical Research (Space*
391 *Physics)*, *118*, 1074-1088. doi: 10.1029/2012JA018343
- 392 Cully, C. M., Bonnell, J. W., & Ergun, R. E. (2008, June). THEMIS obser-
393 vations of long-lived regions of large-amplitude whistler waves in the in-
394 ner magnetosphere. *Geophysical Research Letters*, *35*, L17S16. doi:
395 10.1029/2008GL033643
- 396 Fok, M.-C., Glocer, A., Zheng, Q., Horne, R. B., Meredith, N. P., Albert, J. M., &
397 Nagai, T. (2011, July). Recent developments in the radiation belt environment
398 model. *Journal of Atmospheric and Solar-Terrestrial Physics*, *73*, 1435-1443.
399 doi: 10.1016/j.jastp.2010.09.033
- 400 Glauert, S. A., Horne, R. B., & Meredith, N. P. (2014, January). Three-dimensional
401 electron radiation belt simulations using the BAS Radiation Belt Model with
402 new diffusion models for chorus, plasmaspheric hiss, and lightning-generated
403 whistlers. *Journal of Geophysical Research (Space Physics)*, *119*, 268-289. doi:
404 10.1002/2013JA019281
- 405 Hartley, D. P., Chen, Y., Kletzing, C. A., Denton, M. H., & Kurth, W. S. (2015,
406 February). Applying the cold plasma dispersion relation to whistler mode
407 chorus waves: EMFISIS wave measurements from the Van Allen Probes.
408 *Journal of Geophysical Research (Space Physics)*, *120*(2), 1144-1152. doi:
409 10.1002/2014JA020808
- 410 Hartley, D. P., Kletzing, C. A., Kurth, W. S., Bounds, S. R., Averkamp, T. F.,
411 Hospodarsky, G. B., ... Watt, C. E. J. (2016, May). Using the cold plasma
412 dispersion relation and whistler mode waves to quantify the antenna sheath
413 impedance of the Van Allen Probes EFW instrument. *Journal of Geophysical*
414 *Research (Space Physics)*, *121*, 4590-4606. doi: 10.1002/2016JA022501
- 415 Horne, R. B., Glauert, S. A., Meredith, N. P., Boscher, D., Maget, V., Heynderickx,
416 D., & Pitchford, D. (2013, April). Space weather impacts on satellites and
417 forecasting the Earth's electron radiation belts with SPACECAST. *Space*
418 *Weather*, *11*, 169-186. doi: 10.1002/swe.20023
- 419 Horne, R. B., & Thorne, R. M. (1998). Potential waves for relativistic electron
420 scattering and stochastic acceleration during magnetic storms. *Geophysical Re-*
421 *search Letters*, *25*, 3011-3014. doi: 10.1029/98GL01002
- 422 Horne, R. B., Thorne, R. M., Shprits, Y. Y., Meredith, N. P., Glauert, S. A.,
423 Smith, A. J., ... Decreau, P. M. E. (2005, September). Wave acceleration
424 of electrons in the Van Allen radiation belts. *Nature*, *437*, 227-230. doi:
425 10.1038/nature03939
- 426 Jaynes, A. N., Baker, D. N., Singer, H. J., Rodriguez, J. V., Loto'aniu, T. M.,
427 Ali, A. F., ... Reeves, G. D. (2015, September). Source and seed popu-
428 lations for relativistic electrons: Their roles in radiation belt changes.
429 *Journal of Geophysical Research (Space Physics)*, *120*, 7240-7254. doi:
430 10.1002/2015JA021234
- 431 Kasahara, S., Miyoshi, Y., Yokota, S., Mitani, T., Kasahara, Y., Matsuda, S., ...
432 Shinohara, I. (2018, February). Pulsating aurora from electron scattering by
433 chorus waves. *Nature*, *554*, 337-340. doi: 10.1038/nature25505
- 434 Kletzing, C. A., Kurth, W. S., Acuna, M., MacDowall, R. J., Torbert, R. B.,
435 Averkamp, T., ... Tyler, J. (2013, November). The Electric and Magnetic
436 Field Instrument Suite and Integrated Science (EMFISIS) on RBSP. *Space*
437 *Science Reviews*, *179*, 127-181. doi: 10.1007/s11214-013-9993-6
- 438 Lee, D.-H., Lee, D.-Y., Shin, D.-K., Kim, J.-H., & Cho, J.-H. (2014, December).
439 A Statistical Test of the Relationship Between Chorus Wave Activation and
440 Anisotropy of Electron Phase Space Density. *Journal of Astronomy and Space*
441 *Sciences*, *31*, 295-301. doi: 10.5140/JASS.2014.31.4.295
- 442 Li, W., Bortnik, J., Thorne, R. M., & Angelopoulos, V. (2011, December). Global
443 distribution of wave amplitudes and wave normal angles of chorus waves using

- THEMIS wave observations. *Journal of Geophysical Research (Space Physics)*, 116, A12205. doi: 10.1029/2011JA017035
- Li, W., Santolik, O., Bortnik, J., Thorne, R. M., Kletzing, C. A., Kurth, W. S., & Hospodarsky, G. B. (2016, May). New chorus wave properties near the equator from Van Allen Probes wave observations. *Geophysical Research Letters*, 43, 4725-4735. doi: 10.1002/2016GL068780
- Li, W., Thorne, R. M., Angelopoulos, V., Bortnik, J., Cully, C. M., Ni, B., ... Magnes, W. (2009, May). Global distribution of whistler-mode chorus waves observed on the THEMIS spacecraft. *Geophysical Research Letters*, 36, L09104. doi: 10.1029/2009GL037595
- Li, W., Thorne, R. M., Nishimura, Y., Bortnik, J., Angelopoulos, V., McFadden, J. P., ... Auster, U. (2010, June). THEMIS analysis of observed equatorial electron distributions responsible for the chorus excitation. *Journal of Geophysical Research (Space Physics)*, 115, A00F11. doi: 10.1029/2009JA014845
- Malaspina, D. M., Jaynes, A. N., Boulé, C., Bortnik, J., Thaller, S. A., Ergun, R. E., ... Wygant, J. R. (2016, August). The distribution of plasmaspheric hiss wave power with respect to plasmopause location. *Geophysical Research Letters*, 43, 7878-7886. doi: 10.1002/2016GL069982
- Malaspina, D. M., Jaynes, A. N., Hospodarsky, G., Bortnik, J., Ergun, R. E., & Wygant, J. (2017, August). Statistical properties of low-frequency plasmaspheric hiss. *Journal of Geophysical Research (Space Physics)*, 122, 8340-8352. doi: 10.1002/2017JA024328
- Malaspina, D. M., Ripoll, J.-F., Chu, X., Hospodarsky, G., & Wygant, J. (2018, September). Variation in Plasmaspheric Hiss Wave Power With Plasma Density. *Geophysical Research Letters*, 45, 9417-9426. doi: 10.1029/2018GL078564
- Maxworth, A. S., & Gołkowski, M. (2017, July). Magnetospheric whistler mode ray tracing in a warm background plasma with finite electron and ion temperature. *Journal of Geophysical Research (Space Physics)*, 122, 7323-7335. doi: 10.1002/2016JA023546
- McIlwain, C. E. (1961, November). Coordinates for Mapping the Distribution of Magnetically Trapped Particles. *Journal of Geophysical Research*, 66, 3681-3691. doi: 10.1029/JZ066i011p03681
- Meredith, N. P., Horne, R. B., & Anderson, R. R. (2001, July). Substorm dependence of chorus amplitudes: Implications for the acceleration of electrons to relativistic energies. *Journal of Geophysical Research*, 106, 13165-13178. doi: 10.1029/2000JA900156
- Meredith, N. P., Horne, R. B., Kersten, T., Li, W., Bortnik, J., Sicard, A., & Yearby, K. H. (2018, June). Global Model of Plasmaspheric Hiss From Multiple Satellite Observations. *Journal of Geophysical Research (Space Physics)*, 123, 4526-4541. doi: 10.1029/2018JA025226
- Meredith, N. P., Horne, R. B., Sicard-Piet, A., Boscher, D., Yearby, K. H., Li, W., & Thorne, R. M. (2012, October). Global model of lower band and upper band chorus from multiple satellite observations. *Journal of Geophysical Research (Space Physics)*, 117, A10225. doi: 10.1029/2012JA017978
- Meredith, N. P., Horne, R. B., Thorne, R. M., & Anderson, R. R. (2003, August). Favored regions for chorus-driven electron acceleration to relativistic energies in the Earth's outer radiation belt. *Geophysical Research Letters*, 30, 1871. doi: 10.1029/2003GL017698
- Moldwin, M. B., Downward, L., Rassoul, H. K., Amin, R., & Anderson, R. R. (2002, November). A new model of the location of the plasmopause: CRRES results. *Journal of Geophysical Research (Space Physics)*, 107, 1339. doi: 10.1029/2001JA009211
- Mozer, F. S., Bale, S. D., Bonnell, J. W., Chaston, C. C., Roth, I., & Wygant, J. (2013, December). Megavolt Parallel Potentials Arising from Double-

- 499 Layer Streams in the Earth's Outer Radiation Belt. *Physical Review Letters*,
500 111(23), 235002. doi: 10.1103/PhysRevLett.111.235002
- 501 Orlova, K., Spasojevic, M., & Shprits, Y. (2014, June). Activity-dependent global
502 model of electron loss inside the plasmasphere. *Geophysical Review Letters*, 41,
503 3744-3751. doi: 10.1002/2014GL060100
- 504 Reeves, G., Spence, H. E., Henderson, M. G., Friedel, R. H. W., Funsten, H. O.,
505 Baker, D. N., ... Morley, S. K. (2013, August). Electron Acceleration in
506 the Heart of the Van Allen Radiation Belts. *Science*, 341, 991-994. doi:
507 10.1126/science.1237743
- 508 Santolík, O., Gurnett, D. A., Pickett, J. S., Grimald, S., Décreau, P. M. E., Par-
509 rot, M., ... Fazakerley, A. (2010, August). Wave-particle interactions in the
510 equatorial source region of whistler-mode emissions. *Journal of Geophysical
511 Research (Space Physics)*, 115, A00F16. doi: 10.1029/2009JA015218
- 512 Santolík, O., Gurnett, D. A., Pickett, J. S., Parrot, M., & Cornilleau-Wehrin, N.
513 (2003, July). Spatio-temporal structure of storm-time chorus. *Journal of
514 Geophysical Research (Space Physics)*, 108, 1278. doi: 10.1029/2002JA009791
- 515 Santolík, O., Gurnett, D. A., Pickett, J. S., Parrot, M., & Cornilleau-Wehrin,
516 N. (2005, January). Central position of the source region of storm-time
517 chorus. *Planetary and Space Sciences*, 53(1-3), 299-305. doi: 10.1016/
518 j.pss.2004.09.056
- 519 Santolík, O., Macúšová, E., Kolmašová, I., Cornilleau-Wehrin, N., & Conchy, Y.
520 (2014, April). Propagation of lower-band whistler-mode waves in the outer
521 Van Allen belt: Systematic analysis of 11 years of multi-component data from
522 the Cluster spacecraft. *Geophysical Research Letters*, 41, 2729-2737. doi:
523 10.1002/2014GL059815
- 524 Sazhin, S. S., & Hayakawa, M. (1992, May). Magnetospheric chorus emissions - A
525 review. *Planetary and Space Science*, 40, 681-697. doi: 10.1016/0032-0633(92)
526 90009-D
- 527 Schriver, D., Ashour-Abdalla, M., Coroniti, F. V., LeBoeuf, J. N., Decyk, V.,
528 Travnicek, P., ... Fazakerley, A. N. (2010, August). Generation of whistler
529 mode emissions in the inner magnetosphere: An event study. *Journal of Geo-
530 physical Research (Space Physics)*, 115, A00F17. doi: 10.1029/2009JA014932
- 531 Shi, R., Li, W., Ma, Q., Reeves, G. D., Kletzing, C. A., Kurth, W. S., ... Claude-
532 pierre, S. G. (2017, October). Systematic Evaluation of Low-Frequency Hiss
533 and Energetic Electron Injections. *Journal of Geophysical Research (Space
534 Physics)*, 122, 10. doi: 10.1002/2017JA024571
- 535 Shprits, Y. Y., Subbotin, D. A., Meredith, N. P., & Elkington, S. R. (2008, Novem-
536 ber). Review of modeling of losses and sources of relativistic electrons in the
537 outer radiation belt II: Local acceleration and loss. *Journal of Atmospheric
538 and Solar-Terrestrial Physics*, 70, 1694-1713. doi: 10.1016/j.jastp.2008.06.014
- 539 Subbotin, D. A., & Shprits, Y. Y. (2009, October). Three-dimensional modeling of
540 the radiation belts using the Versatile Electron Radiation Belt (VERB) code.
541 *Space Weather*, 7, S10001. doi: 10.1029/2008SW000452
- 542 Summers, D., Thorne, R. M., & Xiao, F. (1998, September). Relativistic theory
543 of wave-particle resonant diffusion with application to electron acceleration in
544 the magnetosphere. *Journal of Geophysical Research*, 103, 20487-20500. doi:
545 10.1029/98JA01740
- 546 Thorne, R. M. (2010, November). Radiation belt dynamics: The importance of
547 wave-particle interactions. *Geophysical Review Letters*, 37, 22107. doi: 10
548 .1029/2010GL044990
- 549 Tsurutani, B. T., & Smith, E. J. (1977, November). Two types of magnetospheric
550 ELF chorus and their substorm dependences. *Journal of Geophysical Research*,
551 82, 5112-5128. doi: 10.1029/JA082i032p05112
- 552 Tsyganenko, N. A., & Sitnov, M. I. (2005, March). Modeling the dynamics of the in-
553 ner magnetosphere during strong geomagnetic storms. *Journal of Geophysical*

- 554 *Research (Space Physics)*, 110, A03208. doi: 10.1029/2004JA010798
555 Watt, C. E. J., Rae, I. J., Murphy, K. R., Anekallu, C., Bentley, S. N., & Forsyth, C.
556 (2017, September). The parameterization of wave-particle interactions in the
557 Outer Radiation Belt. *Journal of Geophysical Research (Space Physics)*, 122,
558 9545-9551. doi: 10.1002/2017JA024339
559 Wygant, J. R., Bonnell, J. W., Goetz, K., Ergun, R. E., Mozer, F. S., Bale, S. D.,
560 ... Tao, J. B. (2013, November). The Electric Field and Waves Instruments
561 on the Radiation Belt Storm Probes Mission. *Space Science Reviews*, 179,
562 183-220. doi: 10.1007/s11214-013-0013-7